^{9}Be(d, α_0) ^{7}Li (ground state) AND ^{9}Be(d, α_1) ^{7}Li* (470 keV) REACTIONS IN THE 0.9–2.2 MeV ENERGY RANGE

By A. Saganek*, I. Śledzińska* A. Turos**, Z. Wilhelmi* akd B. Zwięgliński**

"Stefan Pieńkowski" Institute of Experimental Physics, University of Warsaw*

and

Institute of Nuclear Research, Warsaw**

(Received December 12, 1970)

Angular distributions and total cross-sections for ^{9}Be$(d, \alpha_0)^7$Li (ground state) and ^{9}Be$(d, \alpha_1)^7$Li* (470 keV) reactions have been measured over the angular range from 15° to 165° (lab.) in 100 keV steps. A detailed description of the experimental technique is given.

The observed behaviour of angular distributions does not allow to determine univocally the dominating reaction mechanism. The revealed features of the reactions in question indicate that these reactions may proceed through overlapping levels of the compound nucleus ^{11}B, which possess opposite parities, and one of them is probably centered at the excitation energy $E_k \approx 17.3$ MeV. However, direct pick-up and heavy particle stripping may be responsible as well.

1. Introduction

Despite many theoretical and experimental efforts, the problem of the interaction mechanism of low energy deuterons with light nuclei has not been so far fully resolved.

Single nucleon transfer reactions — (d, p), (d, n) and (d, t) — often show stripping patterns down to very low energies [1]. The experimental differential cross-sections are quite well described by the distorted wave Born-approximation theory (DWBA), at least in the region of the main stripping peak. The spectroscopic factors thus obtained are in general [1] in agreement with the shell-model calculations [2].

On the other hand, the situation for (d, α) reactions is much less clear [3]. To make some definite conclusions as to the reaction mechanism one needs more data on the angular distributions and excitation functions of these reactions.

The subject of this paper is the experimental investigation of the ^{9}Be$(d, \alpha)^7$Li reactions feding the ground (α_0) and first excited (α_1) states of ^{7}Li in the 0.9–2.2 MeV energy range.

* Address: Instytut Fizyki Doświadczalnej, Uniwersytet Warszawski, Warszawa, Hoża 69, Poland.
** Address: Instytut Badań Jądrowych, Warszawa, Hoża 69, Poland.

The available data on angular distributions and excitation functions of these reactions are listed in Table I. The measurements in the 0.75–2.0 MeV energy range have been performed by Biggerstaff *et al.* [6] with a CsI(Tl) scintillation spectrometer. However, the rather poor energy resolution did not allow for complete resolution of the α_0 and α_1 groups.

Since the angular distributions vary appreciably when crossing the 1–2.5 MeV interval, it seemed worthwhile to repeat the measurements with much better resolution, smaller

TABLE I

Data on the $^9Be(d,\alpha_0)^7Li$ and $^9Be(d,\alpha_1)^7Li$ reactions

Angular distributions

E_d(MeV)	Range of angles (c. m.) covered	Normalization	Reference
0.12	10 –160	rel.	[4]
0.20	0 –170	rel.	[4]
0.30	16 –162	abs.	[5]
0.38	30 –173	rel.	[6]
0.40	27 –162	abs.	[5]
0.43	30 –173	rel.	[6]
0.49	30 –173	abs.	[6]
0.50	32.5 –162	abs.	[5]
0.60	32.5 –162	abs.	[5]
0.70	32.5 –162	abs.	[5]
0.75	32 –165	abs.	[6]
0.80	22 –162	abs.	[5]
0.90	22 –162	abs.	[5]
1.00	32.5 –165	abs.	[6]
1.00	(d,α_0) 33 –162	abs.	[5]
1.00	(d,α_1) 33 –154	abs.	[5]
1.10	34.6 –165	abs.	[6]
1.40	34.6 –165	abs.	[6]
1.58	32 –165	abs.	[6]
1.94	23 –170	abs.	[6]
2.00	34.6 –167.3	abs.	[6]
2.19	34.6 –155	abs.	[6]
2.39	34.6 –155	abs.	[6]

Excitation functions

θ_{lab}	Range of energies (lab) covered	Normalization	Reference
90°	0.88 –2.35	rel.	[6]
100°	0.3 –1.00	abs.	[5]
165°	(d,α_0) 0.5 –1.9	rel.	[6]
165°	(d,α_1) 0.5 –1.6	rel.	[6]

energy steps and, if possible, to extend them to smaller angles. It was anticipated that these factors would facilitate the theoretical analysis and throw some light on the mechanism governing these (d, α) reactions.

2. *Experimental*

a) Accelerator and beam handling

The measurements were made at the Institute of Nuclear Research using a 2.5 MeV Van de Graaff generator. The energy was set with an accuracy higher than ± 10 keV. After bending in the beam-switching magnet the beam was focused at the center of the scattering chamber (see Fig. 1) by means of two quadrupole lenses. These lenses permit also to displace the beam in the vertical and horizontal directions to compensate some errors in the ion optics.

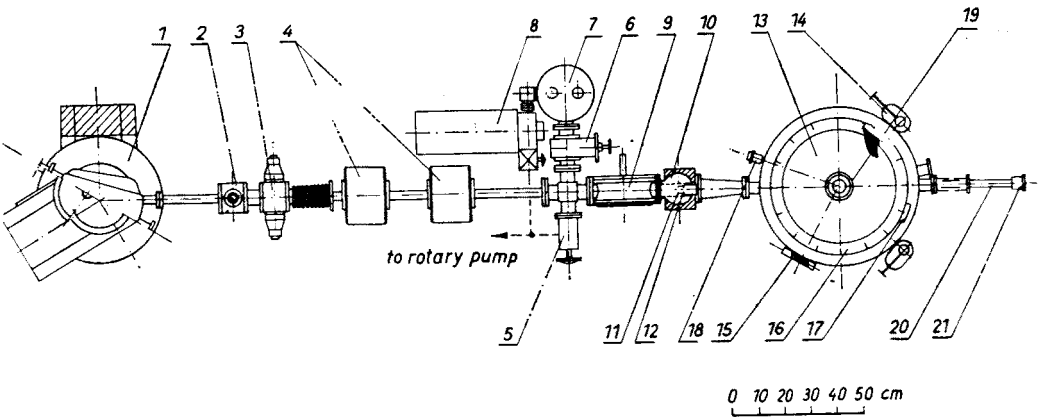

Fig. 1. Experimental setup: *1* — beam-switching magnet, *2* — quartz viewer, *3* — stabilizing slits, *4* — quadrupole lenses, *5* — roughing vacuum valve, *6* — gate valve, *7* — oil diffusion pump with liquid nitrogen cold trap, *8* — low vacuum tank, *9* — beam viewer, *10* — rotary connector, *11* — first collimating slit and quartz disc with a hole, *12* — antiscattering slit, *13* — scattering chamber, *14* — vertical and horizontal setting screws, *15* — worm gear, *16* — dial, *17* — vernier, *18* — monitor housing, *19* — foil assembly, *20* — Faraday cup, *21* — quartz viewer

The beam enters the scattering chamber through a collimator formed by two tantalum slits with circular openings. The first entrance slit to the collimator has a diameter of 2.2 mm. It is followed by an antiscattering slit with a slightly larger diameter which prevents the particles scattered on the edges of the first defining slit from entering the chamber. The second defining slit placed at a distance of 35 cm from the entrance slit has a diameter of 2.8 mm. The collimator limits the angular divergence of the deuteron beam at the center of the chamber to $\pm 25'$, and the dimensions of the beam spot on the target to 3.1 mm. After passing through the target material the beam is collected in a Faraday cup.

The chamber is connected to the beam tube by means of a rotary spherical connector with the first defining slit, mentioned above, located in its center. A quartz disc with a hole in its center is clamped to the surface of this slit. The position of the beam spot on the quartz

disc may be observed from the outside through a viewing window. Such an arrangment facilitates greatly the initial alignment of the chamber.

b) Scattering chamber

The scattering chamber has an inner diameter of 30 cm and the distance between the top and bottom lids is 10 cm (see Fig. 2).

The top lid carrying the detector housing is rotated by means of a worm gear to change the detector angle. The angular position of the detector can be set with an accuracy of $\pm 0.25°$ by means of a dial and a vernier. The top lid rests on three ball bearings which facilitate greatly rotation when the chamber is under vacuum.

The detector looks at the beam spot on the target through two circular slits of 2.2 mm diameter 3.0 cm apart. A small magnet is located between them to prevent the electrons ejected from the target material from reaching the sensitive volume of the detector (see Fig. 3 for details). The distance between the detector defining slit and the chamber axis which could be varied continuously was set in the measurements reported below at 11 cm. The acceptance angle of the detector at the adopted geometry of the slits was $\pm 0.6°$.

The zero angle on the dial was set optically and checked by Coulomb scattering. The 1.8 MeV deuteron beam was scattered on a thin gold target, and the asymmetry of scattering was measured at equal angles on both sides of the beam. The asymmetry never exceeded $\pm 1.8\%$.

To be able to shift the energies of some of the measured particles with respect to others, the scattering chamber was equipped with an energy degrading device (see Fig. 2). Five replacable aluminium foils of different thickness are fastened to the rotary arm. Each of them may be placed before the detector slits.

The housing of the monitor detector is clamped rigidly to the side surface of the chamber. This detector is also equipped with a pair of slits. The axis of the collimator thus formed is set at 157.5° to the beam direction and inclined at an angle of 15° to the reaction plane.

The target rod with the target holder is centered on the vertical axis of the chamber. The target holder may carry five targets simultaneously, and by changing the vertical position of the holder it is possible to introduce any single target into the beam. The angle of inclination of the target surface relative to the beam direction can be continuously varied and observed on the dial.

c) Targets

Most of the measurements were made using beryllium targets with thin organic backings. Spectroscopically pure beryllium was evaporated in vacuum from a tantalum boat onto glass slides preliminarily coated with an acetone solution of polyvinyl acetate. The targets thus prepared can be easily stripped from the glass when placed in warm, distilled water. They were then picked-up on target frames, dried and mounted on the target holder.

The beryllium layer of the targets used in this experiment was about 15 keV thick (at 2 MeV deuteron energy). The organic backing withstands prolonged bombardment with currents up to 0.15 μA.

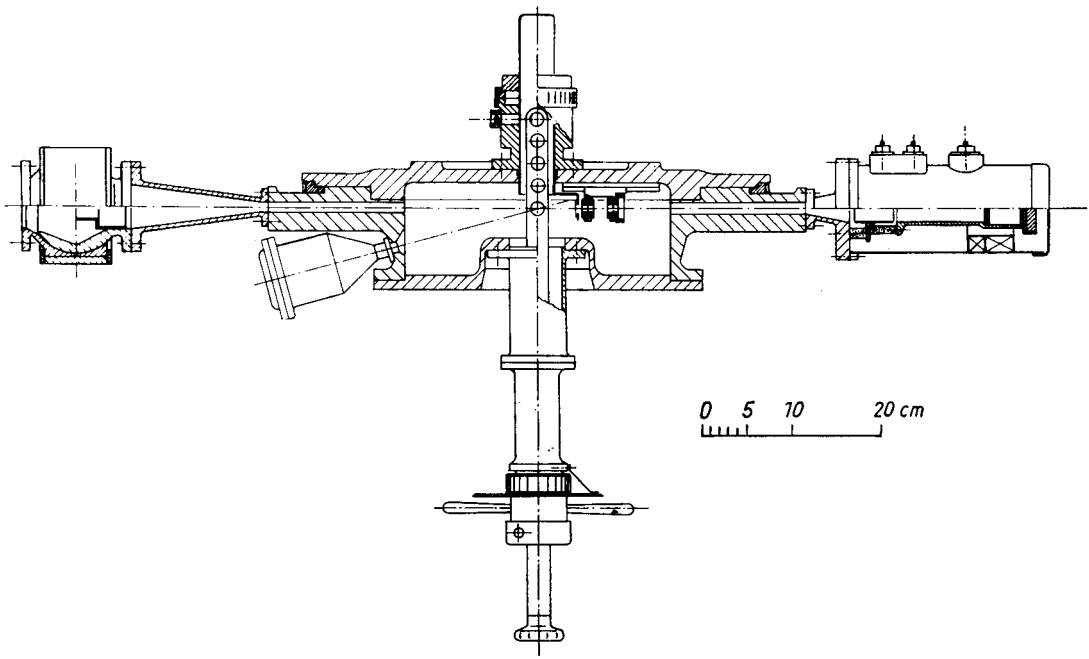

Fig. 2. Scattering chamber

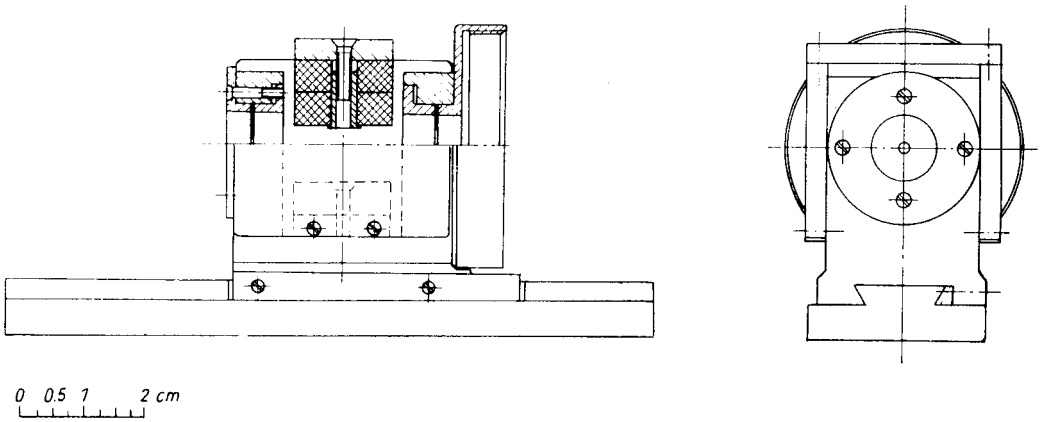

Fig. 3. Detector mounting

Some of the measurements had to be performed with targets containing a minimum amount of carbon. Aluminium oxide (Al_2O_3) backings of 1000 Å thickness were then used, prepared by anodic oxidation of aluminium foils.

d) Detectors and electronics

Semiconductor detectors of the surface barrier type were used to measure the spectra of charged particles. They were fabricated of 5000 ohm. cm silicon in this laboratory [7]. The detectors were connected to the low noise (3.5 keV) charge sensitive preamplifiers of conventional design.

After amplification, the pulses were separately analysed and stored by two "Intertechnique" analyzers: the spectra from the monitor detector by the 400 channel SA-40-B analyzer, and those from the main detector by the 1024 channel CA 25/BM 96 analyzer.

It was necessary to take great care to avoid errors in experimental angular distributions due to the "dead-time" losses in the analyzers. The counting rate of the monitor analyzer never exceeded 5–10 pulses per second and its "dead-time" was negligible. On the other hand, the counting rate of the main detector varied substantially when going from backward to forward angles, where almost all the cross-sections attain their maximum values. To compensate the "dead-time" losses in the main analyzer, the gate of the monitor analyzer was turned-off whenever the "dead-time" pulse appeared at the output of the main analyzer, informing that this one is in its "busy" cycle.

3. Results

a) General

A typical charged particle spectrum obtained at $E_d = 2.1$ MeV and $\theta_{lab} = 50°$ with beryllium target with a thin organic backing is shown in Fig. 4. The spectra of particles from the $^{12}C(d, p)$ reactions on a pure carbon target and $^{16}O(d, p)$ reactions on an Al_2O_3 target measured under identical conditions were used for energy calibration and peak identification. The 60 keV half-width of the α-group shown in the figure is representative for most of the measured spectra.

Beside the α_0 and α_1 groups, an alpha-particle group feeding the particle-unstable 4.63 MeV state of ^{7}Li is clearly visible in the spectrum. From the reaction kinematics (Fig.5) it may be seen that this group coincides at some angles with ^{7}Li recoils and/or $^9Be(d, p_1)$ and $^{16}O(d, p_1)$ groups, and therefore the measurements of the 4.63 α-group have not been undertaken. Starting with 5.5 MeV, downwards, the continuum of particles is observed. It is composed of tritons feeding the broad ($\Gamma \approx 1.5$ MeV) first excited state of ^{8}Be and/or tritons and alphas from the decay of particle unstable states of both ^{8}Be and ^{7}Li.

At some angles the α_0 and α_1 groups have energies identical to the energy of the $^{13}C(d, \alpha_0)$ group (see Fig. 5) originating from carbon contained in the target backing. However, it was not attempted to correct the final results for its presence, the error connected with this effect being of the order of 1% only.

When the bias voltage of the detector is lowered, the $^9Be(d, p_0)^{10}Be$ (ground state) protons leave only a small fraction of their energy in the sensitive volume. The α_0 and α_1 groups, having a much shorter range, are completely stopped and separated from protons of the same energy (see Fig. 5) in the measured spectra.

Coulomb scattering of deuterons in the target materials sets a lower limit on forward angles (15°) reached in this experiment. A random summing of alpha-pulses and deuteron pulses in the circuitry ("pile-up" effect) increasingly smears the alpha-groups when angles are decreased. It was possible to perform the measurements in the region 15°–30° only when the ion current was as low as 0.02 μA and an aluminium stopping foil of 5 μm thickness was placed before the counter. Nevertheless, the resolution obtained in this interval is

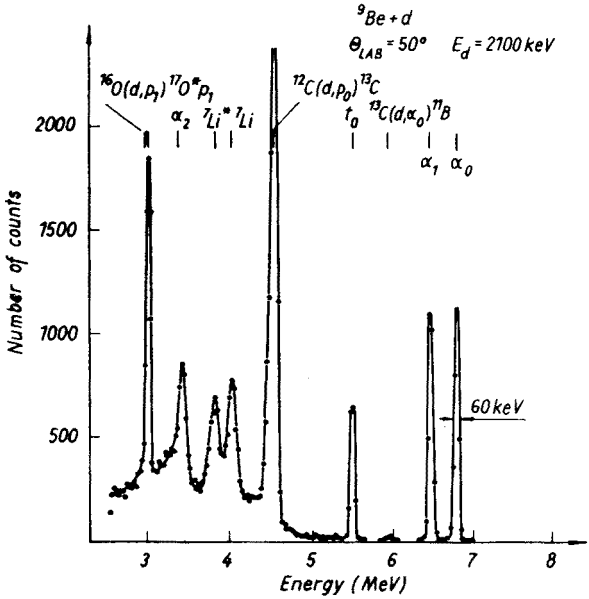

Fig. 4. Spectrum of particles measured at $E_d = 2.1$ MeV and $\theta_{\text{lab}} = 50°$

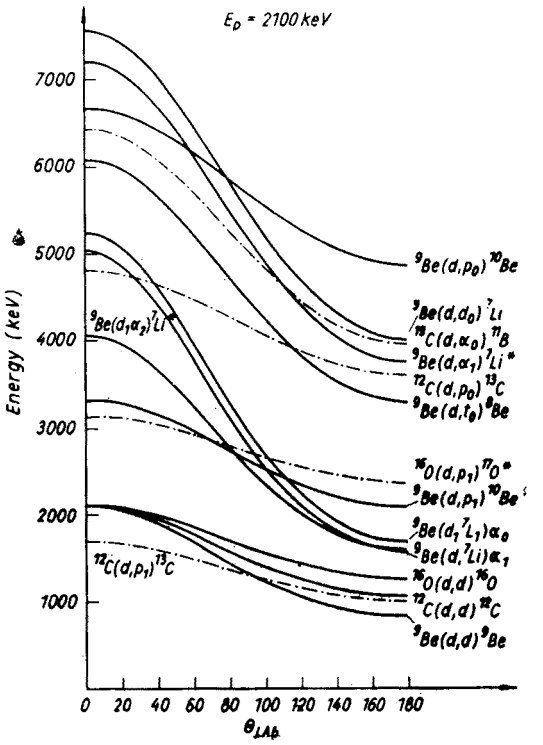

Fig. 5. Reaction kinematics at $E_d = 2.1$ MeV

poorer than that quoted above as typical for all other angles, and a uniform background appears under the peaks.

At each deuteron energy the spectra at 150° (lab.) or 120° (lab.) were measured without the low energy cutoff so as to contain the ^{9}Be(d, d) elastic scattering peak. Fig. 6 illustrates the way the background under the elastic peak was subtracted. The known elastic scattering cross-sections [8] were used to establish the absolute values of the (d, α) cross-sections. The 150° normalization was adopted in most cases. At $E_d = 1300$ keV and 1400 keV the proximity of the ^{12}C(d, p_1) peak made the measurements of the ^{9}Be(d, d) scattering at 150° difficult.

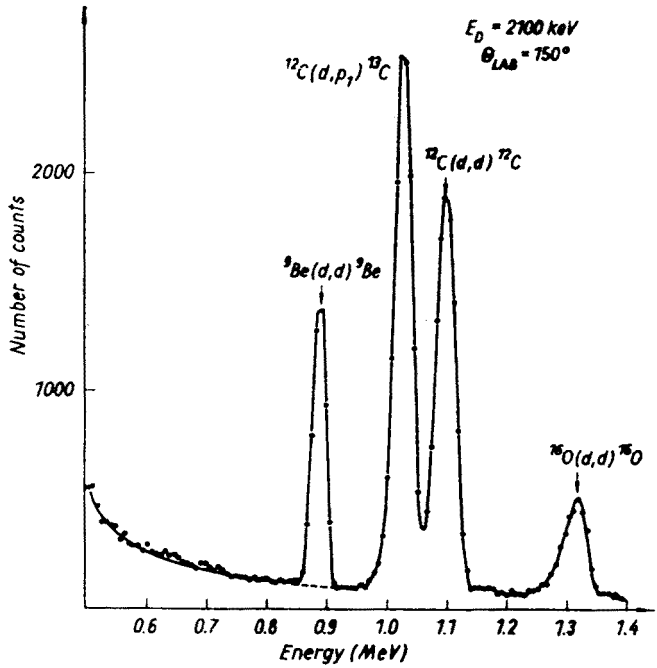

Fig. 6. Low energy part of spectrum measured at $E_d = 2.1$ MeV and $\theta_{\text{lab}} = 150°$

The angular distributions of α-particles were measured in the deuteron energy range 0.9–2.2 MeV in 100 keV steps. The experimental points cover the region of angles 40°–165° (lab.) at 10° intervals and the region 15°–40° at 5° intervals.

The graphs of the angular distributions for the ^{9}Be(d, α_0) and ^{9}Be(d, α_1) reactions in the center of mass system are shown in Figs 7 and 7*a*, and Figs 8 and 8*a*, respectively. The solid curves represent the least-squares fits of the experimental points with the sum of Legendre polynomials up to the seventh order. The fitted curves give a smooth extrapolation of the data beyond the measured region. The (d, α) total cross-sections shown in Fig. 9 are based on these fits.

The numerical values of the differential and total cross-sections are given in Ref. [9], and are available from the authors on request.

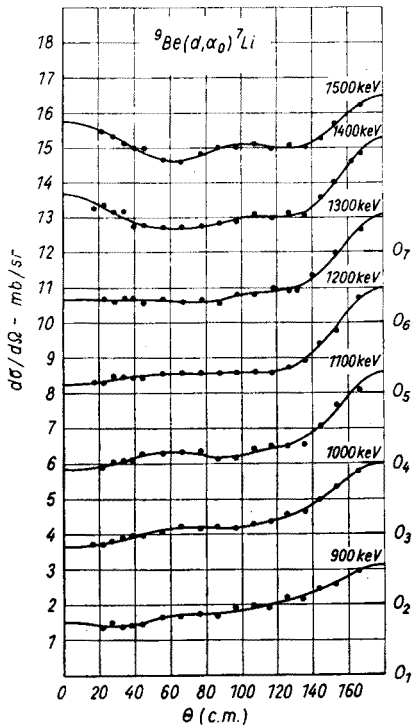

Fig. 7

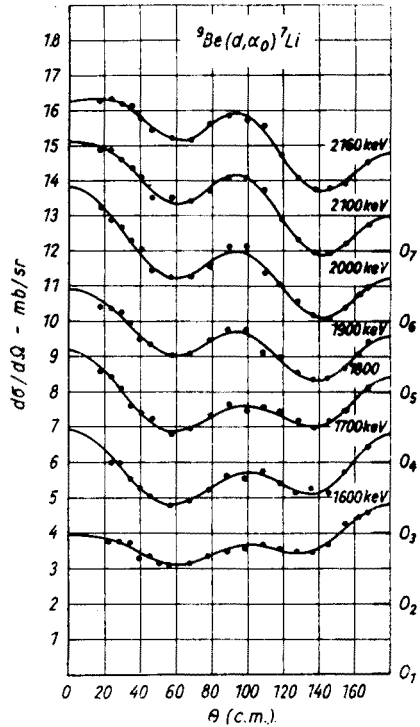

Fig. 7a

Fig. 7. Angular distributions of the $^9Be(d, \alpha_0)^7Li$ (ground state) particles in the 0.9–1.5 MeV energy range. Solid lines passing through the experimental points represent the Legendre-polynomial fits

Fig. 7a. Angular distributions of the $^9Be(d, \alpha_0)^7Li$ (ground state) particles in the 1.6–2.2 MeV energy range. Solid lines passing through the experimental points represent the Legendre-polynomial fits

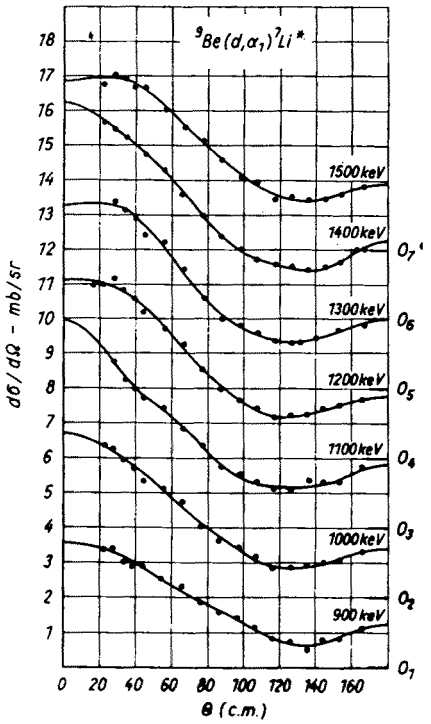

Fig. 8

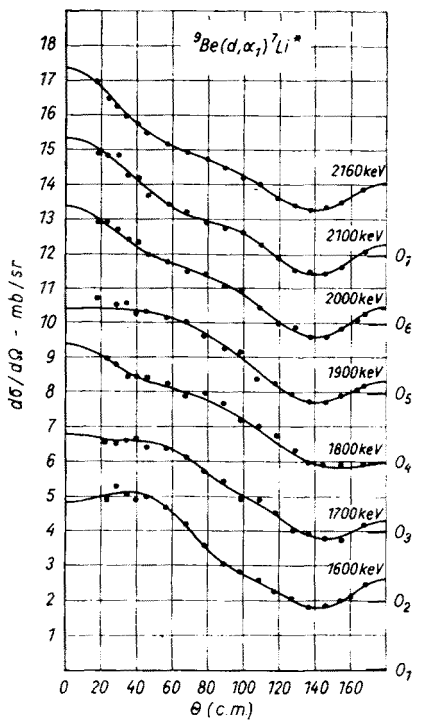

Fig. 8*a*

Fig. 8. Angular distributions of the $^9Be(d,\alpha_1)^7Li^*$ (1-st exc. state) particles in the 0.9–1.5 MeV energy range Solid lines passing through the experimental points represent the Legendre-polynomial fits

Fig. 8*a*. Angular distributions of the $^9Be(d,\alpha_1)^7Li^*$ (1-st exc. state) particles in the 1.6–2.2 MeV energy range. Solid lines passing through the experimental points represent the Legendre-polynomial fits

b) Errors

In Figs 7 and 8 the error bars represent only the statistical errors of the measurements, which do not exceed $\pm 3\%$. The presence of the background under the peaks at forward angles (15°–30° lab.) adds some systematical errors, the accurate values of which are difficult to assess. This background was subtracted and only the peak area taken into account in our data. Since some α-pulses "piled-up" with deuterons may be contained therein, it cannot be excluded that the cross-sections at forward angles are underestimated.

Taking into account all the possible sources of errors both systematical and statistical, it may be stated that the overall errors of the absolute (d,α) cross-sections do not exceed $\pm 10\%$ inclusive of the uncertainty of 5% of the elastic scattering cross-sections [8]. Most of the results agree to within $\pm 20\%$ with those of Biggerstaff *et al.* [6], well within the limits of errors stated in the two works. The largest discrepancies appear at forward angles and lowest energies for reasons discussed above.

4. *Discussion*

The main feature of the angular distributions presented in Figs 7, 7*a*, and 8, 8*a* is their relatively weak energy dependence.

The ^{9}Be$(d, \alpha_1)^7$Li reaction preserves its forward peaked character throughout the entire energy range. Forward peaking, less distinct at lowest energies, increases gradually, while the position of the minimum cross-section remains fixed at $\theta_{\text{c.m.}} \approx 135°$. The incident energy variations affect to a larger extent the (d, α_0) cross-sections. At lowest energies (0.9–1.3 MeV) they are flat, and only starting with $\theta_{\text{c.m.}} \approx 135°$ they rise more rapidly towards $\theta_{\text{c.m.}} = 180°$. When the bombarding energy is further increased, the (d, α_0) angular distributions show a distinct oscillatory modulation, and the whole pattern "rotates" clockwise around the $\theta_{\text{c.m.}} \approx 135°$ point, so that at highest energies the angular distributions become forward peaked. Somewhere between 1.8 and 1.9 MeV it assumes the shape approximately symmetric with respect to $\theta_{\text{c.m.}} \approx 90°$.

These trends are reflected in the energy dependence of the coefficients of the Legendre polynomial expansion:

$$d\sigma(E_d, \theta)/d\Omega = \frac{\sigma_t(E_d)}{4\pi}\left(1 + \sum_{K=1}^{K_{\max}} a_K(E_d) P_K(\cos\theta)\right) \tag{1}$$

where $d\sigma(E_d, \theta)/d\Omega$ is the differential cross-section at the deuteron energy E_d and c.m.s. angle θ, $\sigma_t(E_d)$ is the total reaction cross-section at E_d, $P_K(\cos\theta)$ is the Legendre polynomial of the order K, $K_{\max}$ being the maximum order of the polynomial needed to be taken into account to reproduce the experimental differential cross-sections.

An automatic search programme [10] was used to find the values of the parameters σ_t and a_K's giving the minimum χ^2 value between the experimental points and formula (1). χ^2 is defined as usually:

$$\chi^2 = \frac{1}{N}\sum_{i=1}^{N}\left\{\frac{[d\sigma(\theta_i)/d\Omega]_{\text{exp}} - [d\sigma(\theta_i)/d\Omega]_{\text{th}}}{\Delta\sigma(\theta_i)}\right\}^2 \tag{2}$$

where N is the number of experimental points, $[d\sigma(\theta_i)/d\Omega]_{\text{exp}}$ is the experimental differential cross-section at θ_i, $[d\sigma(\theta_i)/d\Omega]_{\text{th}}$ is the theoretical cross-section given by (1), $\Delta\sigma(\theta_i)$ is the probable error of the measurement at θ_i.

The first seven polynomials were used in the fitting procedure. The coefficients in the above expansion are plotted as a function of energy in Figs 9, 10 and 11. The upper indices 0 and 1 refer to the ground and first excited state transitions, respectively. The error bars indicate the uncertainties in the coefficients due to the statistical errors in the data.

The gross features of the energy dependence of the ^{9}Be$(d, \alpha_0)^7$Li (ground state) angular distributions are contained in the energy dependence of the isotropic (σ_t), a_1^0 and a_4^0 terms and to smaller extent in the remaining ones. The negative value of the a_1^0 term is responsible for the tendency to falling towards zero degrees at lowest energies (0.9–1.0 MeV). When a_1^0 crosses zero at $E_d = 1.8$ MeV the angular distribution is almost symmetric with respect to 90°and when a_1^0 rises further to positive values the angular distributions acquire a forward

peaked character. The important modulation, mentioned above, is caused by the a_4^0 term, which increases gradually throughout the entire energy range.

On the other hand, the (d, α_1) can be satisfactorily fitted by a smaller number of Legendre polynomials. The isotropic (σ_t^1), a_1^1 and a_2^1 are the dominating ones up to 1.8 MeV, where a_4^1 also must be taken into account. The strongly forward peaked shape of (d, α_1) is connected with large, positive values of the a_1^1 term. The a_1^1 and a_2^1 coefficients show a broad anomaly centred at *ca* 1.8 MeV.

Most striking is the fact, that the two transitions possess almost identical total cross sections (see Fig. 9), in spite of the seemingly different behaviour of their angular distributions.

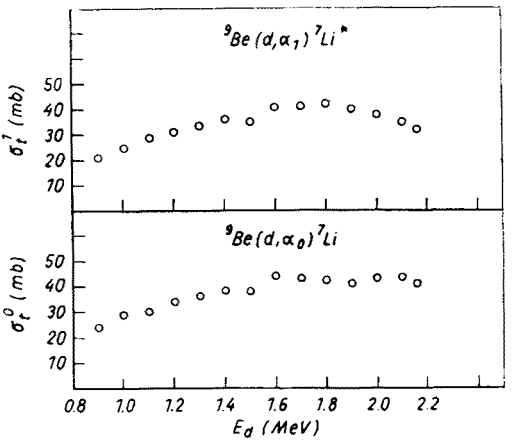

Fig. 9. Total $^9Be(d, \alpha_0)^7Li$ and $^9Be(d, \alpha_1)^7Li^*$ cross-sections in the 0.9–2.2 MeV energy range

In the range of bombarding energies covered in this experiment the compound nucleus ^{11}B, if such is formed, would be excited from 16.56 to 17.62 MeV. If there existed an isolated level of the compound nucleus, it would give angular distributions symmetric with respect to $\theta_{c.m.} = 90°$, *i.e.* only Legendre polynomials of even order would contribute. Its decay, if not inhibited by some selection rules dictated by the peculiarities of the intrinsic structure, would be almost instantaneous due to the large decay energy available in all opened channels (numerous neutron and a few proton and triton channels are open beside the (d, α) ones). It is, thus plausible to expect that the level in question will be large and may overlap and interfere with other levels lying nearby. The presence of strong a_1^0 and a_1^1 terms indicates the existence of interference effects between the compound levels of opposite parities. The fact that (d, α_0) assumes an almost symmetric shape at $E_d \approx 1.85$ MeV may indicate the location of the compound level of ^{11}B with an excitation energy of 17.3 MeV. It is worth stressing that these interference effects persist down to the lowest energy ($E_d = 0.12$ MeV) at which these reactions were investigated [4], well below the Coulomb barrier. The existence of a_1 terms at such a low energy indicates the presence of the deuteron p-wave (and/or higher partial wave) interaction, which may be amplified by a resonance level located sufficiently close to the 15.82 MeV ^8Be+d threshold in ^{11}B.

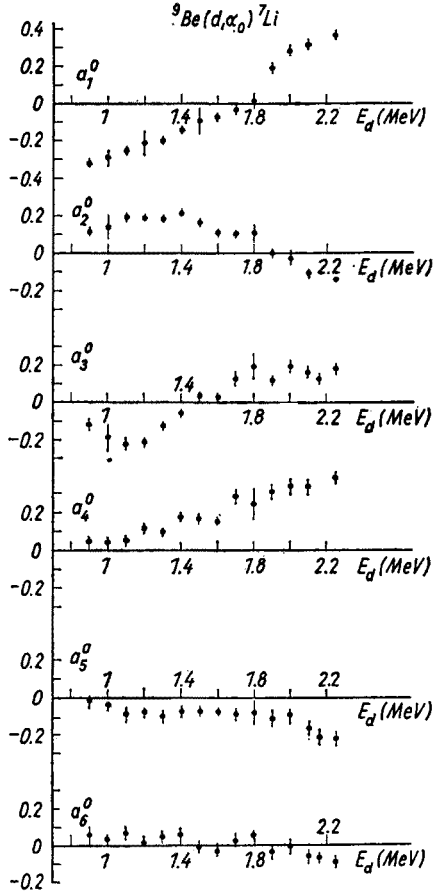

Fig. 10

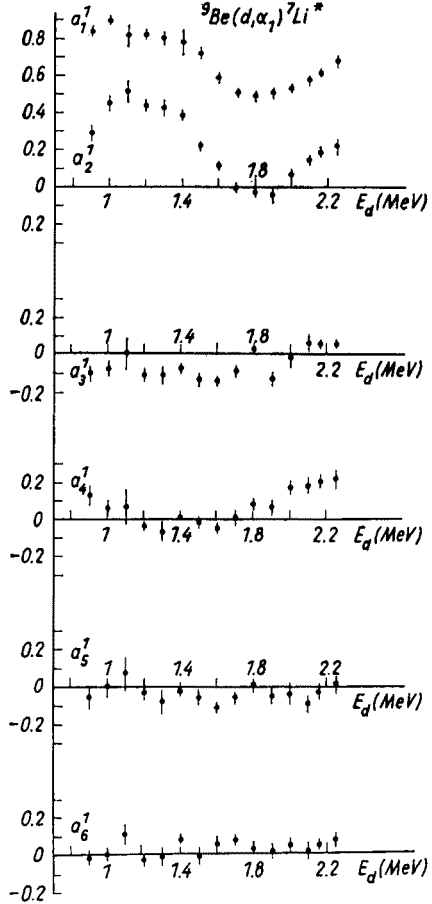

Fig. 11

Fig. 10. Legendre polynomial coefficients for the $^9Be(d, \alpha_0)^7Li$ reaction as a function of incident deuteron energy. The error bars indicate the uncertainties in the coefficients due to the statistical errors in the data

Fig. 11. Legendre polynomial coefficients for the $^9Be(d, \alpha_1)^7Li^*$ reaction as a function of incident deuteron energy. For error bars see caption to Fig. 10

Some features of the reactions such as the discussed above relatively smooth energy dependence and distinct forward peaking of (d, α_1) deserve a direct interaction approach. Three ways of the direct one-step transition between the initial and final channels are usually taken into account in (d, α) reactions:

1. The incident deuteron may pick-up the deuteron cluster from the target nucleus to form the outgoing α-particle (pick-up mechanism).

2. It may knock-out an alpha-particle from the target, being captured itself to form the final state of the residual nucleus (knock-out mechanism).

3. The target nucleus may undergo stripping. In our case the ^{5}He cluster is transferred from the target to the deuteron (heavy-particle stripping — HPS).

Pick-up and knock-out mechanism give forward peaked angular distributions, while HPS backward peaked ones. The dispersion theory of direct nuclear reactions [11] predicts the dominance of these reaction mechanisms, whose Feynman graphs have poles lying closest to the physical region. In our case the distance of pick-up and HPS poles from the physical region equals 95 MeV·a.m.u., while the knock-out pole is 212 MeV·a.m.u. distant. It may therefore be concluded that the former two ought to dominate.

Before applying the full DWBA treatment it seemed worth-while to analyse the angular distributions according to the simplest plane wave theory of Newns [12]. In terms of this theory angular distributions have the form of squares of the absolute values of the Bessel functions:

$$\frac{d\sigma}{d\Omega} \sim \sum_L b_L |j_L(KR)|^2. \tag{3}$$

Where L is the orbital angular momentum quantum number and has different meanings for the pick-up and HPS mechanism, K is the absolute value of momentum transfer at a given c.m.s. angle, and R is the interaction radius. The summation goes over all L-values compatible with angular momentum and parity conservation; $L = 0$ and 2 in our case. The radii R and the weights are treated as fitting parameters.

The best fit to the ^{9}Be$(d, \alpha_1)^7$Li angular distribution at $E_d = 0.9$ MeV gave, assumming a pure pick-up mechanism, the interaction radius $R = 3$ fm, and the weights of $L = 0$ and $L = 2$ components equal to 1 and 0.5 respectively.

An independent fit to ^{9}Be$(d, \alpha_0)^7$Li at the same energy gave, assuming pure HPS mechanism, $R = 3$ fm and equal weights of the $L = 0$ and $L = 2$ terms. The fitted curves and experimental points are shown in Figs 12 and 13 for the (d, α_0) and (d, α_1) transitions, respectively.

It is expected that the inclusion of a coherent mixture of the two mechanisms may account for the experimental data throughout the entire energy range. It should be added, however, that at higher energies similar plane wave fits to the (d, p) and (d, t) reactions on ^{9}Be have given interaction radii of the order of 4–4.5 fm. If a direct interaction really occurs in our (d, α) reactions, the cause of this large difference is difficult to explain.

In this section some qualitative features of the ^{9}Be(d, α) reactions were stressed, which may be interpreted in terms of mutually contradictory compound nucleus and direct interaction mechanisms. Further quantitative analysis will show which of them gives more

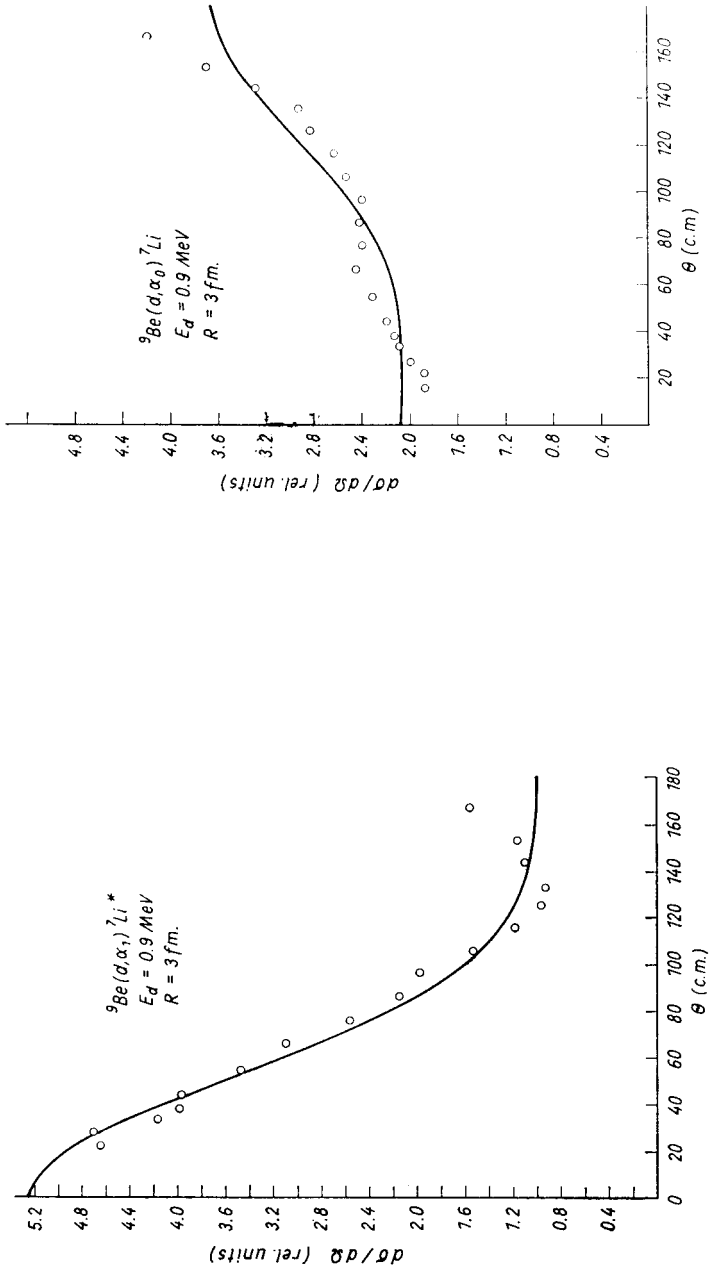

Fig. 13

Fig. 12

Fig. 12. Angular distribution of the $^9\mathrm{Be}(d,\alpha_0)^7\mathrm{Li}$ reaction at $E_d = 0.9$ MeV. The solid line is calculated from the Newns' plane wave formula, assuming a HPS mechanism (further details in text)

Fig. 13. Angular distribution of the $^9\mathrm{Be}(d,\alpha_1)^7\mathrm{Li}^*$ at $E_d = 0.9$ MeV. The solid line is calculated from the Newns' plane wave formula assuming a pick-up mechanism (further details in text)

consistent results. This analysis is now in progress and its results shall be published in due course.

The authors are greatly indebted to Drs F. Machali, Z. A. Saleh, A. T. Baranik, F. Asfour, I. Boundouk and V. E. Storizhko for supplying the numerical values of the elastic cross-sections.

Besides the authors' sincere gratitude is due to Dr M. Jaskóła and the Van de Graaff staff for their able operation of the accelerator, and to Dr H. Rękawek and his collaborators for the help in the design and construction of the scattering chamber. The high quality of the semiconductor detectors supplied by Dr A. Marcinkowski's group is greatly appreciated and the help of Mrs R. Sochacka in the target preparation is gratefully acknowledged.

REFERENCES

[1] R. H. Siemssen, M. Cosack, R. Felst, *Nuclear Phys.*, **69**, 209 (1965); A. Gallmann, P. Fintz, P. E. Hodgson, *Nuclear Phys.*, **82**, 161 (1966); P. E. Hodgson, D. Wilmore, *Proc. Phys. Soc.*, **90**, 361 (1967); O. Dietzsch, R. A. Douglas, E. Farrelly Pessoa, V. Gomes Porto, E. W. Hamurger, T. Polga, O. Sala, S. M. Perez, P. E. Hodgson, *Nuclear Phys.*, **A114**, 330 (1968) H. Beaumevielle, M. Lambert, M. Yaker, A. Amokrane, Nguyen Van Sen, *Nuclear Phys.*, **A125**, 568 (1969); V. Gomes Porto, N. Ueta, R. A. Douglas, O. Sala, D. Wilmore, B. A. Robson, P. E. Hodgson, *Nuclear Phys.*, **A136**, 385 (1969).

[2] M. H. Macfarlane, J. B. French, *Rev. Mod. Phys.*, **32**, 567 (1960).

[3] M. N. H. Comsan, M. A. Farouk, A. A. El-Kamhawy, M. S. M. El-Tahawy, A. N. Lvov, *Atomkernenergie*, **13**, 415 (1968); I. I. Żalubovskii, A. P. Lobkovskii, G. L. Vysockii, *Izv. Akad. Nauk SSSR* (ser. fiz), **33**, 2057 (1969); S. W. Cosper, B. T. Lucas, O. E. Johnson, *Phys. Rev.*, **139**, B763 (1965); V. Gomes Porto, N. Ueta, R. A. Douglas, O. Sala, D. Wilmore, B. A. Robson, P. E. Hodgson, *Nuclear Phys.*, **A136**, 385 (1969).

[4] G. Ambrosino, J. P. Crettez, J. Lachkar, J. Perchereau, *J. Phys. Suppl.*, C1–62 (1966).

[5] F. Bertrand, G. Grenier, J. Pornet, *Report CEA-R*-3504 (1968), unpublished.

[6] J. A. Biggerstaff, R. F. Hood, H. Scott, M. T. Mc Ellistrem, *Nuclear Phys.*, **36**, 631 (1962).

[7] T. Czyżewski, A. Kamiński, A. Marcinkowski, A. Modelska-Berkan, *Post. Techn. Jądr.*, **11**, 614 (1967), in Polish.

[8] F. Machali, Z. A. Saleh, A. T. Baranik, F. Asfour, L. Boundouk, V. E. Storizhko, *Atomkernenergie*, **13**, 29 (1968).

[9] A. Saganek, I. Śledzińska, A. Turos, Z. Wilhelmi, B. Zwięgliński, *Report INR*-1200/I/PL, Warsaw 1970, unpublished.

[10] W. Grochulski, W. Wójcik, *Report INR*-866/I/PL, Warsaw 1967, unpublished.

[11] I. S. Shapiro, in *Selected Topics in Nuclear Theory*, ed. International Atomic Energy Agency, Vienna 1963.

[12] H. C. Newns, *Proc. Phys. Soc.*, **76**, 489 (1960).